

NAND-like SOT-MRAM-based approximate storage for error-tolerant applications

Min Wang^{1,†}, Zhengyi Hou^{1,†}, Chenyi Wang^{1,†}, Zhengjie Yan¹, Shixing Li¹, Ao Du¹, Wenlong Cai¹,
Jinhao Li¹, Hongchao Zhang¹, Kaihua Cao¹, Kewen Shi¹, Bi Wang¹, Yuanfu Zhao², Qingyi
Xiang³, Zhaohao Wang^{1,*}, and Weisheng Zhao¹

¹School of Integrated Circuit Science and Engineering, Beihang University, Beijing, China

²Beijing Microelectronics Technology Institute, Beijing, China

³Huawei Technologies Co., Ltd, Shenzhen, China

[†]authors contributed equally

*corresponding author: zhaohao.wang@buaa.edu.cn

Abstract

We demonstrate approximate storage based on NAND-like spin-orbit torque (SOT) MRAM, through “device-modeling-architecture” explorations. We experimentally achieve down to 1E-5 level selectivity. Selectivity and low-power solutions are established by numerical calculation workflow. System-level power consumption is evaluated in the 512 KB last-level cache according to 5 quality levels. Error-tolerant applications, such as image processing, alleviate the demand for selectivity down to the 5E-2 level, leading to 54% ~ 61% energy-saving. Our proposal paves the novel and suitable path for high-density and low-power NAND-like SOT-MRAM.

1 Introduction

Emerging NAND-like SOT devices employ the structure of multiple bits arranged in the same SOT track [1–3], which features area saving and high efficiency, but requires low-error-rate selective operation through modulation effect, e.g., spin transfer torque (STT) or voltage-controlled magnetic anisotropy (VCMA) effect. In-plane anisotropy (IMA) SOT-MTJ holds the field-free switching mechanism, the back-end of line (BEOL) compatibility, and radiation tolerance [4–7]. However, pursuing the desired selectivity, e.g., 1E-6 level, requires high energy consumption and a strong modulation effect. Here, we propose and demonstrate that approximate storage relaxes the requirement of selectivity for NAND-like SOT devices and thus achieves significant energy-saving.

2 Experiment and results

We first fabricate 4-bit NAND-like SOT devices based on a 200-mm-wafer manufacturing platform with MgO(1.5 nm), noted as Process A (Fig. 1(a) and (b)) [7]. Negative vertical voltage ($-V_M$) assists writing in IMA devices, as verified by micromagnetic simulation (Fig. 1(c)) and experiments (Fig. 2(b)-(d)) [2]. Statistics of TMR versus MTJ position and canted angles are listed in Fig. 2(a). Fig. 2(b)-(d) summarizes the switching probability (P_{sw}) and critical switching SOT voltage (V_{sw}) for various cases. Critical SOT current density is inferred as 11.9 MA/cm²@300 ns. An available window exists in the 1E-5 level selectivity by electrical measurement (Fig. 3(a)). Under the “ballooning”, the selectivity of most devices is limited to the 1E-3 ~ 1E-4 level, which fortunately does not limit their use as approximate storage. In addition, excessively high selectivity targets may lead to endurance problems (Fig. 3(b)). Fig. 4 shows the results of the two test methods, under the fixed V_M or fixed V_{TOP} . Different control voltages should be designed for 4 MTJs to achieve better modulation, especially in μm -level tracks (Fig. 4(b)), due to the position-dependent IR drop along the SOT track. In addition, Process B prepared sub-100 nm devices (MgO~1.1 nm), and Fig. 5 shows the results at 5 ns pulses.

3 Modeling and workflow

The numerical calculation workflow (Fig. 6) is established by considering (i) equivalent temperature assumption, (ii) temperature dependence of parameters, (iii) magnetoresistance modeling, etc [8,9]. The results for a single bit (Fig. 7(a)) are in good agreement with the experimental characteristics (Fig. 5). The contribution factors of STT and VCMA (c_{STT} and c_{VCMA}) can be further estimated. The dominant role gradually shifts from STT to VCMA with thicker MgO, as shown in Fig. 7(b).

4 Solutions for selectivity

In Fig. 8, energy evaluation is performed assuming a miniaturized track and 1E-2 level selectivity (i.e., approximate storage). As shown in Fig. 8(a), the required VCMA coefficient ξ decreases with thinner MgO, transitioning from the voltage-controlled to the current-controlled mechanism. The former has the advantage of ultra-low energy consumption (55.6 fJ@99% P_{sw} and 1.7 nm MgO), noted as Solution A. Fig. 8(b) provides another possible way to balance energy consumption and requirement for ξ . An increase in pulse width causes a decrease in controlling voltage, forming a local optimum at ~ 20 ns pulse width (153 fJ@99% P_{sw}), noted as Solution B.

5 Image processing application

As shown in Fig. 9(a), two 4-bit NAND-like SOT devices are utilized as the high-significance and low-significance bits (HSB and LSB) for 8-bit image data approximate storage. Fig. 9(b) illustrates the workflow for satisfying different quality requirements by using the writing voltage and LSB as the quality knob. Fig. 9(c) shows the distribution of energy consumption in the 512 KB last-level cache. The device parameters for 5 quality levels (L1-L5) are listed in Table.1. The JPEG and Sobel processing outputs are shown in Fig. 10. As shown in Fig. 11(a), the results of root mean square error (RMSE) in L1-L4 are more acceptable compared with L5. Fig. 11(b) illustrates that $\sim 61\%$ and $\sim 54\%$ energy-saving are achieved from L1 to L4 for Solutions A and B, respectively. According to Table.2, the proposed approaches have a 40 to 323 times writing energy decrease than reported works [10], with RMSE less than 30.

6 Conclusion

Our work demonstrates the BEOL compatibility, low power consumption, and adaptability of multi-terminal operation in arrays for NAND-like SOT devices. In image processing, NAND-like SOT devices serve as approximate storage with less requirement for selectivity (5E-2 level is enough) and 54% \sim 61% energy-saving from L1 to L4. Overall, our proposal opens up new application scenarios and opportunities for SOT-MRAMs.

Acknowledgements

This work was supported by the National Natural Science Foundation of China under Grant 62171013, 62271026, and 62104015, National Key Research and Development Program of China (Nos. 2021YFB3601303, 2021YFB3601304).

References

- [1] K. Cai, S. Van Beek, S. Rao, K. Fan, M. Gupta, V. Nguyen, G. Jayakumar, G. Talmelli, S. Couet, and G. S. Kar, "Selective operations of multi-pillar SOT-MRAM for high density and low power embedded memories," in *2022 IEEE Symposium on VLSI Technology and Circuits (VLSI Technology and Circuits)*, pp. 375–376, IEEE, 2022.
- [2] T. Inokuchi, H. Yoda, Y. Kato, M. Shimizu, S. Shirotori, N. Shimomura, Y. Kamiguchi, H. Sugiyama, S. Oikawa, K. Ikegami, *et al.*, "Improved read disturb and write error rates in voltage-control spintronics memory (VoCSM) by controlling energy barrier height," *Applied Physics Letters*, vol. 110, no. 25, 2017.
- [3] K. Shi, W. Cai, Y. Zhuo, D. Zhu, Y. Huang, J. Yin, K. Cao, Z. Wang, Z. Guo, Z. Wang, *et al.*, "Experimental demonstration of NAND-like spin-torque memory unit," *IEEE Electron Device Letters*, vol. 42, no. 4, pp. 513–516, 2021.

- [4] B. Wang, M. Wang, H. Zhang, Z. Wang, Y. Zhuo, X. Ma, K. Cao, L. Wang, Y. Zhao, T. Wang, *et al.*, “Ionization and displacement damage on nanostructure of spin-orbit torque magnetic tunnel junction,” *IEEE Transactions on Nuclear Science*, vol. 69, no. 1, pp. 43–49, 2021.
- [5] A. Du, D. Zhu, K. Cao, Z. Zhang, Z. Guo, K. Shi, D. Xiong, R. Xiao, W. Cai, J. Yin, *et al.*, “Electrical manipulation and detection of antiferromagnetism in magnetic tunnel junctions,” *Nature Electronics*, vol. 6, no. 6, pp. 425–433, 2023.
- [6] H. Honjo, T. Nguyen, T. Watanabe, T. Nasuno, C. Zhang, T. Tanigawa, S. Miura, H. Inoue, M. Niwa, T. Yoshiduka, *et al.*, “First demonstration of field-free SOT-MRAM with 0.35 ns write speed and 70 thermal stability under 400°C thermal tolerance by canted SOT structure and its advanced patterning/SOT channel technology,” in *2019 IEEE International Electron Devices Meeting (IEDM)*, pp. 28–5, IEEE, 2019.
- [7] H. Zhang, X. Ma, C. Jiang, J. Yin, S. Lyu, S. Lu, X. Shang, B. Man, C. Zhang, D. Li, *et al.*, “Integration of high-performance spin-orbit torque MRAM devices by 200-mm-wafer manufacturing platform,” *Journal of Semiconductors*, vol. 43, no. 10, p. 102501, 2022.
- [8] V. Krizakova, E. Grimaldi, K. Garelo, G. Sala, S. Couet, G. S. Kar, and P. Gambardella, “Interplay of voltage control of magnetic anisotropy, spin-transfer torque, and heat in the spin-orbit-torque switching of three-terminal magnetic tunnel junctions,” *Physical Review Applied*, vol. 15, no. 5, p. 054055, 2021.
- [9] T. Taniguchi, S. Isogami, Y. Shiokawa, Y. Ishitani, E. Komura, T. Sasaki, S. Mitani, and M. Hayashi, “Magnetization switching probability in the dynamical switching regime driven by spin-transfer torque,” *Physical Review B*, vol. 106, no. 10, p. 104431, 2022.
- [10] A. M. H. Monazzah, A. M. Rahmani, A. Miele, and N. Dutt, “Cast: Content-aware STT-MRAM cache write management for different levels of approximation,” *IEEE Transactions on Computer-Aided Design of Integrated Circuits and Systems*, vol. 39, no. 12, pp. 4385–4398, 2020.

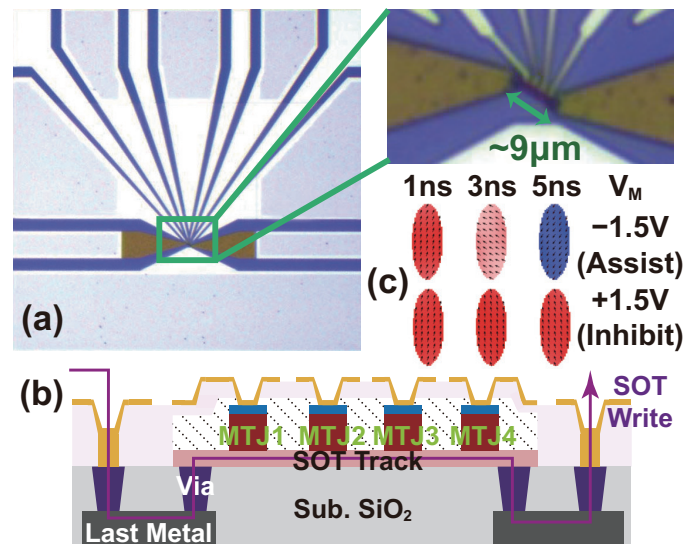


Figure 1: (a) Microscopy image and (b) schematic of the 4-bit NAND-like SOT device. (c) Micromagnetic simulation under various V_M .

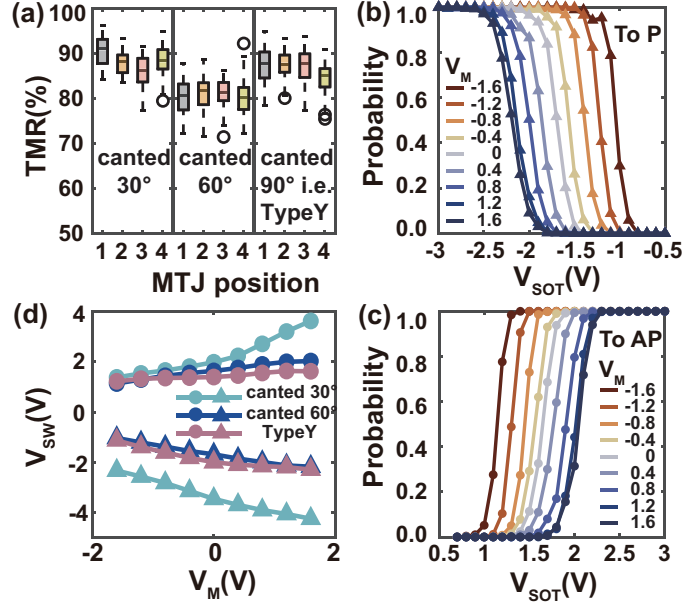


Figure 2: (a) TMR statistics (over 16 dies). Switching probability P_{sw} versus V_M during (b) P and (c) AP writing at 300 ns pulse. (d) Voltage modulation at various types of devices.

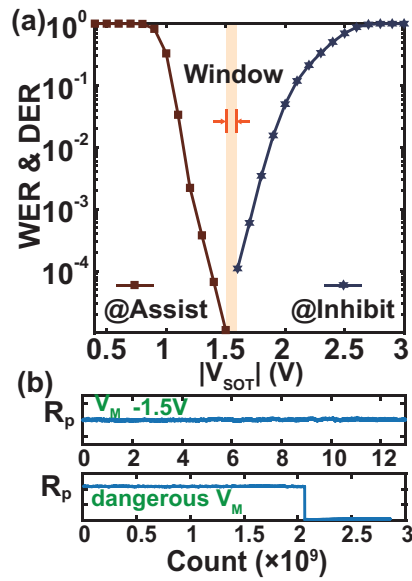


Figure 3: (a) $1E-5$ level selectivity@500 ns. (b) Case of breakdown (MgO ~ 1.3 nm)

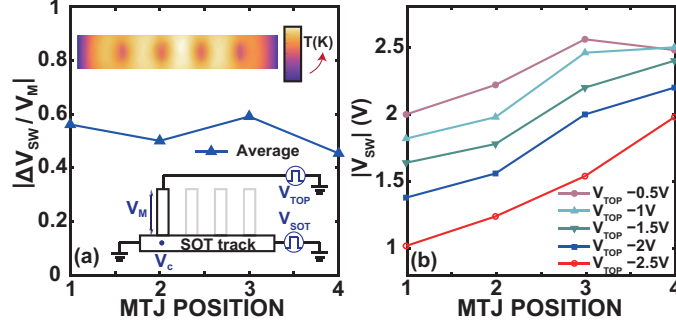


Figure 4: Experimental results for MTJ at various positions in 4-bit NAND-like devices. (a) Average $|\Delta V_{sw}/V_M|$ under the same $\pm V_M$ in bipolar writing. Inset is the temperature distribution on the SOT track by Multiphysics simulation. (b) Dependence of $|V_{sw}|$ on the V_{TOP} and MTJ positions.

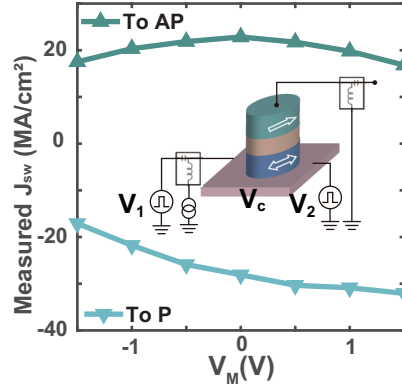


Figure 5: Experimental results of J_{sw} @ 5 ns as a function of V_M in Process B, with J_{SOT} assumed as $\min\{J_{SOT}(V_1, V_c), J_{SOT}(V_c, V_2)\}$

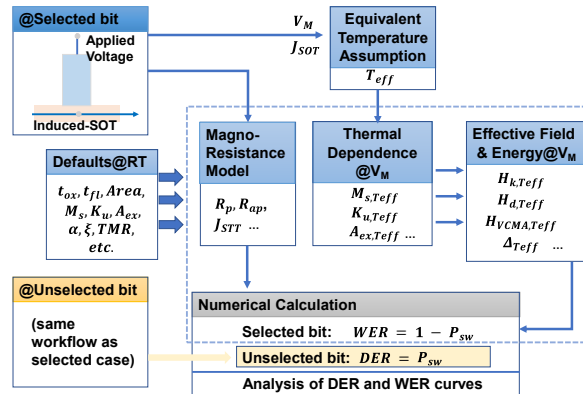


Figure 6: Numerical calculation workflow for modulation and selectivity analysis.

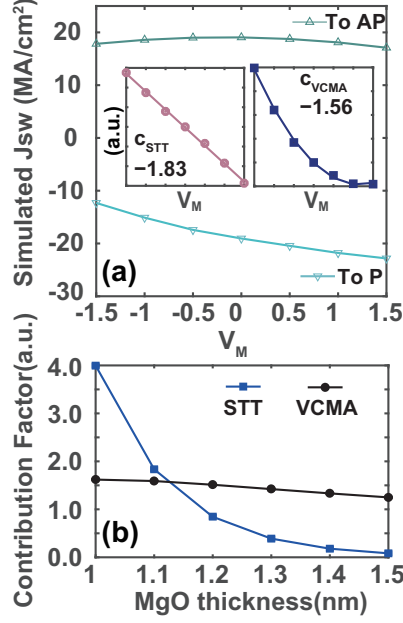


Figure 7: (a) J_{sw} as a function of V_M . (b) c_{STT} and c_{VCMA} in various MgO thicknesses. Normalized $j_{sw} = 1 - (\pm c_{STT}V_M + c_{VCMA}V_M + c_TV_M^2)/|J_{sw,0}|$.

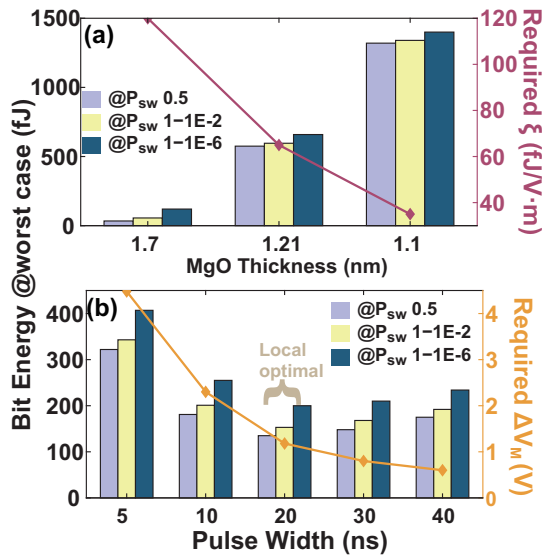


Figure 8: Energy consumption @ worst bit and (a) required ξ at different MgO thicknesses t_{ox} while fixing ΔV_M to 3 V (e.g., ± 1.5 V). (b) required ΔV_M under various pulse widths while fixing ξ to 60 fJ/(V·m) and t_{ox} to 1.4 nm.

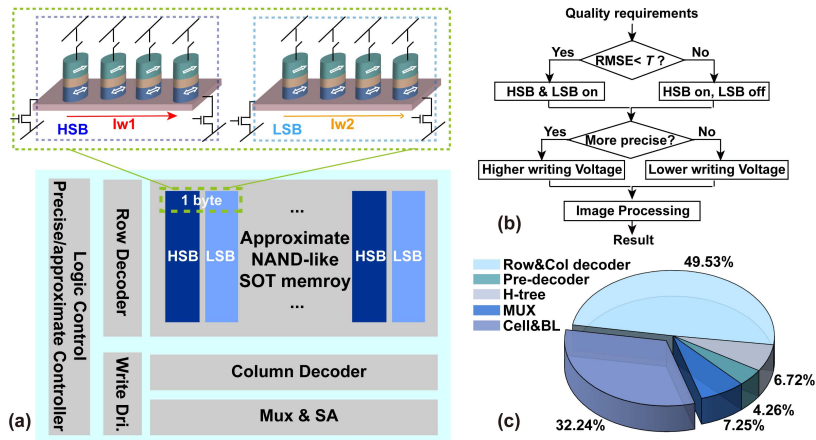


Figure 9: NAND-like SOT-based approximate storage concept. (a) The proposed structure and the 1-byte data cell with 4 bits HSB and 4 bits LSB. (b) The proposed workflow satisfies different quality requirements, where T denotes the user-defined threshold. (c) Distribution of the energy consumption in a 512 KB approximate storage last-level cache.

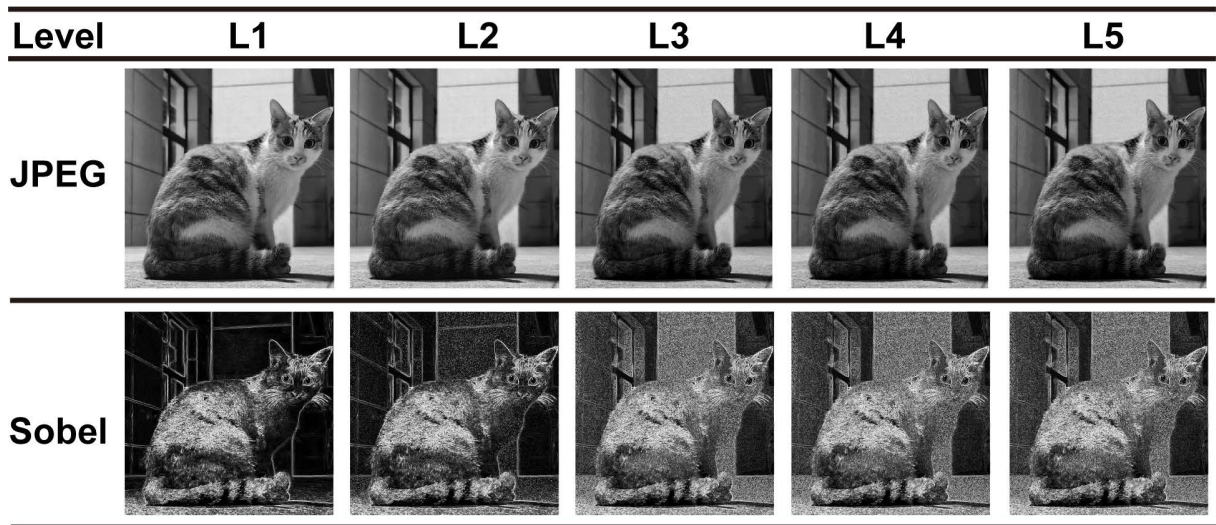


Figure 10: Output of JPEG and Sobel for 5 quality levels.

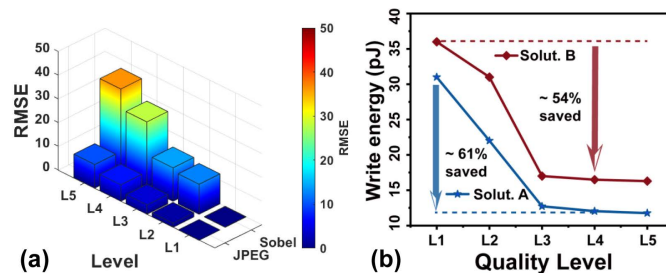


Figure 11: (a) RMSE results in different image processing applications, and (b) write dynamic energy consumption for an 8-byte cache line of two approaches.

Table 1: Quality-Energy map for NAND-like devices. P_{sw} and write average energy per bit are obtained by calculation workflow.

Quality Level		L1(baseline)	L2	L3	L4	L5
$P_{sw}(\%)$	HSB	99.9999	99	99	95	90
	LSB	99.9999	99	0	0	0
$E_{write}(\text{fJ})$	Solution A	119	54.7	54.7	45.6	41.9
	Solution B	192	146	146	137	134

Table 2: Performance comparison.

Technology	QuARK [10]	CAST [10]	This work	
	STT-MRAM	STT-MRAM	NAND-like SOT-MRAM	
Quality knob	V_{STT}	V_{STT}	Solution A	Solution B
$E_{write}(\text{pJ})$ @worst case*	672.25	5325	12.04	16.48
Energy-saving(%)	47	69	61	54
RMSE @worst case	31.93	31.93	27.95	

* E_{write} is reported for an 8-byte cache line, L4 is acceptable worst case.